Influence of Site-Specific Sulfonation on Acrylic Graft Copolymer Morphology

Tomonori Saito,[†] Brian D. Mather,[†] Philip J. Costanzo,[§] Frederick L. Beyer,[‡] and Timothy E. Long*,[†]

Department of Chemistry, Macromolecules and Interfaces Institute, Virginia Tech, Blacksburg, Virginia 24061-0212; Army Research Laboratory, Materials Division, Aberdeen Proving Ground, Aberdeen, Maryland 21005-5069; and Department of Chemistry & Biochemistry, California Polytechnic State University, San Luis Obispo, California 93407

Received January 24, 2008; Revised Manuscript Received March 11, 2008

ABSTRACT: Novel selectively sulfonated graft copolymers, poly(methyl methacrylate)-*g*-(poly(sulfonic acid styrene)-*b*-poly(*tert*-butylstyrene)), poly(methyl methacrylate)-*g*-(poly(*tert*-butylstyrene)-*b*-poly(styrenesulfonic acid)), and the corresponding sodium sulfonate salts were successfully synthesized. The weight-average molecular weights (M_w) of the graft copolymers were ∼200 000 g/mol and the polydispersity ranged from 1.86 to 2.22. The graft copolymers contained ∼9−10 branches on average and 4 wt % of sulfonic acid or sodium sulfonate blocks adjacent to the backbone or at the branch terminus. The mobility of the sulfonated blocks located at the branch terminus enabled the sulfonated blocks to more readily interact and form ionic aggregates. The glass transition temperatures of the sulfonated graft copolymer with sulfonated blocks at the branch terminus were higher than values for copolymers with sulfonated blocks adjacent to the backbone. This behavior was attributed to the sulfonated blocks at the branch terminus more easily forming ionic aggregates. In general, appearance of multiple scattering maxima in the small-angle X-ray scattering (SAXS) data indicated the formation of lamellar morphologies. More facile aggregation of sulfonated blocks at the branch terminus resulted in the appearance of ionomer peaks in SAXS whereas ionomer peaks were not observed in sulfonated graft copolymers with sulfonated blocks adjacent to the backbone. Reasonable fits of the Yarusso−Cooper model to the SAXS data strongly supported the identification of the nonlamellar maxima as ionomer peaks. Strong ionic interactions with Na^+ counterions reduced the Bragg spacings, d, of the sodium sulfonate graft copolymers and increased the size of the ionic aggregates. The location of sulfonated blocks in both sulfonic acid and sodium sulfonate graft copolymers significantly affected thermal properties and morphologies.

Introduction

Graft copolymers enable a wide variety of emerging applications due to their unique macromolecular architecture. Understanding intra- and intermolecular interactions in graft copolymers is crucial for tuning the functionality and performance of graft copolymers. Well-defined synthesis and characterization of graft copolymers are necessary to understand their unique structure−property relationships.[1] A generally accepted strategy for obtaining more well-defined branched polymers involves copolymerization of macromonomers with backbone-forming monomers. A macromonomer is defined as a functional oligomer with a polymerizable end group.[2] The chain length of the macromonomer, which defines the length of branches in the graft copolymer, is predetermined and precisely controlled using living polymerization strategies. The choice of monomers and the order of monomer addition also control the composition of the branch and backbone upon subsequent copolymerization.[3]

Block copolymers, graft copolymers, and ionomers often exhibit microphase separation, and this morphological control dramatically influences the physical properties of the polymer. Occurrence of microphase separation depends on many factors, including compositional dissimilarity, molecular weight, and crystallizability.[4] The Flory−Huggins binary segmental interaction parameter, χ, describes the degree of the enthalpic interactions between components. The volume fraction of the component and $\chi N/\lambda$, where N is the degree of polymerization and λ is the number of branches per graft copolymer, predict the phase behavior of graft copolymer systems.[5]

Gido and co-workers[6,7] demonstrated the utility of the constituting block copolymer hypothesis in their studies on several graft copolymers. The graft copolymers possessed either regularly spaced tetrafunctional branch points[6] or randomly placed trifunctional and tetrafunctional branch points.[7] The morphological behavior of the regularly spaced graft copolymers supported the constituting block copolymer hypothesis, in which smaller architectural subunits of the graft copolymers dictated the morphological behavior of the large complex architectures of graft copolymers.[6] Graft copolymers with randomly placed branch points also followed the constituting block copolymer hypothesis but exhibited less well-ordered morphologies than analogues with regularly spaced branch points.[7]

Holdcroft et al. synthesized graft copolymers containing ionic polymer grafts (poly(styrenesulfonic acid) graft chains) attached to a hydrophobic backbone.[8,9] Their macromonomer strategy resulted in uniform graft chain length of the poly(styrenesulfonic acid) branches. They studied the thermal, morphological, and proton exchange properties. This study provided insight into the importance of a well-defined graft copolymer in determining and understanding the structure−property relationships. Although this class of ionomeric graft copolymers is suitable for studying structure−property relationships, due to the challenging synthesis of well-defined ionomers, the relationship between structure and morphology of branched polymers remains as a challenge.

We are interested in the structure−property relationships of multiphase ionomers as a function of the relative location of sulfonated blocks. The location of sulfonated blocks in branched architecture is expected to affect various properties. Understand-

* Corresponding author. E-mail: telong@vt.edu.
[†] Virginia Tech.
[‡] Aberdeen Proving Ground.
[§] California Polytechnic State University.

10.1021/ma800178d CCC: $40.75
Published on Web 04/17/2008

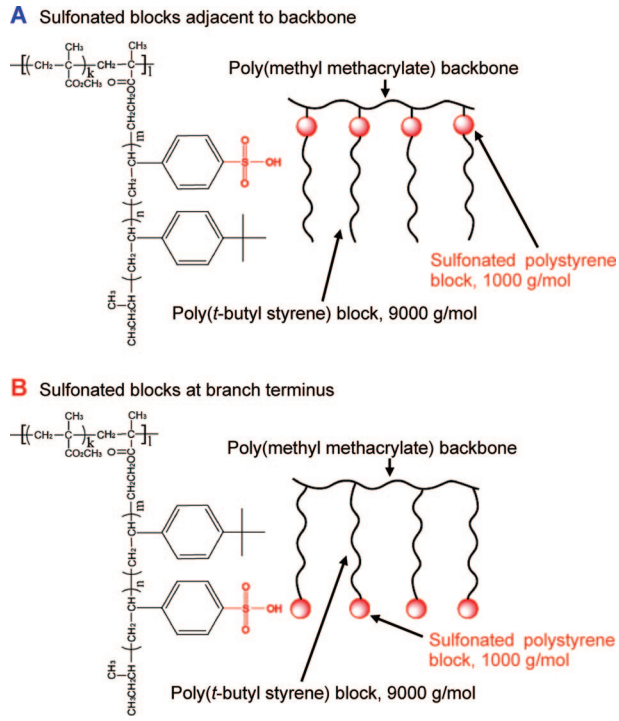

Figure 1. Chemical structures and schematic images of the site-specifically sulfonated graft copolymers.

ing this fundamental concept may provide important insight for macromolecular design and property tuning. Researchers have predicted that the distribution of sulfonated groups along the backbone, acid strength, and the relative location to the polymer backbone have a considerable effect on the final morphology and properties.[10] However, because of synthetic difficulties, most synthetic methods that are utilized to form acid- and ion-containing polymers such as proton exchange membranes have resulted in random or statistical placement of sulfonic acid units along the copolymer chain.[10,11] Thus, a fundamental study of the structure−property relationships with well-defined branched sulfonated ionomers has only received sparse attention.

This paper describes site-specifically sulfonated graft copolymers, which leads to the elucidation of structure−property relationships of sulfonated graft copolymers as a function of the relative location of sulfonated blocks. The structures and schematic representations of the site-specifically sulfonated graft copolymers are shown in Figure 1. The synthetic methodology that was utilized for controlled graft copolymer synthesis with precise location of sulfonated blocks involved preformed macromonomers.[12] Poly(*tert*-butylstyrene)-*b*-polystyrene (P*t*BS-*b*-PS) diblock macromonomers were synthesized via living anionic polymerization. The diblock macromonomer contained 1000 g/mol polystyrene and 9000 g/mol poly(*tert*-butylstyrene). The macromonomer ensured controlled molecular weight and distribution of the graft. P*t*BS-*b*-PS diblock macromonomers were subsequently copolymerized with methyl methacrylate (MMA). Polystyrene blocks were site-specifically sulfonated as the *tert*-butyl group hindered sulfonation of the poly(*tert*-butylstyrene) blocks.[13–19] The sulfonated blocks were placed either adjacent to the backbone, which will be referred to as A, or at the branch terminus, which will be referred to as B. In this paper, we will discuss the synthesis of well-defined site-specifically sulfonated graft copolymers and thermal and morphological characterization of the sulfonated graft copolymers using differential scanning calorimetry (DSC), small-angle X-ray scattering (SAXS), and transmission electron microscopy (TEM) as a function of relative location of sulfonated blocks.

Experimental Section

Materials. Styrene (Aldrich, 99%) and *tert*-butylstyrene (Scientific Polymer Products, 95%) were dried over calcium hydride (Aldrich, 95%) for 24 h and distilled under vacuum. The monomers were treated with an aliquot of dibutylmagnesium (Aldrich, 1.0 M) and distilled under vacuum prior to use. Cyclohexane (Burdick & Jackson, HPLC) was passed through an activated molecular sieve column (Aldrich, 60 Å mesh) and activated alumina column immediately prior to use. Methacryloyl chloride (Aldrich, 96%) was distilled under nitrogen. Triethylamine (Aldrich, 99%) was stirred over calcium hydride (Aldrich, 95%) and distilled under vacuum. Methyl methacrylate (MMA, 98%, Aldrich) was deinhibited via passing through activated basic alumina column. *sec*-Butyllithium (Aldrich, 1.4 M), ethylene oxide (Aldrich, 99.98%), 2,2-azobis(isobutyronitrile) (AIBN, 99%, Aldrich,) dichloroethane (Aldrich, 99%), acetic anhydride (Aldrich, 98%), and sulfuric acid (Aldrich, 98%) were used as received.

Synthesis of Hydroxy-Terminated Poly(*tert*-butylstyrene-*block*-styrene). A 500 mL capacity anionic polymerization reactor was filled with cyclohexane (350 mL), and the temperature was maintained at 50 °C. *tert*-Butylstyrene (44.12 mL, 39.00 g) was syringed into the reactor. *sec*-Butyllithium (3.961 mL, 4.333 mmol) was then added to the solution to initiate anionic polymerization. As illustrated in Scheme 1, reaction 1, the first reaction was allowed to proceed 1 h and the second monomer, styrene (4.767 mL, 4.333 g), was added. After 1 h of polymerization, ethylene oxide was bubbled through the reaction solvent for 2 min and then terminated by adding acidified methanol. The diblock copolymer was precipitated into methanol, and the recovered polymer was dried at 100 °C in vacuum for 24 h. Synthesis of γ-hydroxypoly(styrene-*block*-*tert*-butylstyrene) was also performed by exchanging the order of first block (*tert*-butylstyrene) and the second block (styrene) addition. ^{1}H NMR (400 MHz, $CDCl_3$, δ): 0.6−0.8 ppm (br, $CH_3CH_2CH(CH_3)-$), 0.9−2.5 ppm (br, $-CH_2-$, $-CH_2CH-$, $-C(CH_3)_3$ in polystyrene and poly(*tert*-butylstyrene) units), 3.2−3.4 ppm (br, $-CH_2CH_2OH$), 6.0−7.3 ppm (br, aromatic protons in polystyrene and poly(*tert*-butylstyrene) units).

Functionalization of Hydroxy-Terminated Diblock Copolymers to Methacrylate Macromonomers. γ-Hydroxypoly(*tert*-butylstyrene-*block*-styrene) (36.60 g) was dissolved in THF (350 mL). Triethylamine (3.014 mL, 18.94 mmol) was syringed into the reaction vessel. After cooling to 0 °C, methacryloyl chloride (1.683 mL, 17.22 mmol) in THF (10 mL) was added dropwise. The reaction proceeded for 18 h with warming to room temperature. The macromonomer was precipitated into isopropyl alcohol, and the recovered polymer was dried at 50 °C in vacuum for 24 h. The reaction scheme is shown in Scheme 1, reaction 2. ^{1}H NMR (400 MHz, $CDCl_3$, δ): 0.6−0.8 ppm (br, $CH_3CH_2CH(CH_3)-$), 0.9−2.5 ppm (br, $-CH_2-$, $-CH_2CH-$, $-C(CH_3)_3$, $CH_2{=}C(CH_3)-$), 3.7−4.1 ppm (br, $-CH_2CH_2OCO-$), 5.5 ppm (d, J = 17.2 Hz, $CH_{trans}H{=}C(CH_3)-$), 5.9 ppm (d, J = 17.2 Hz, $CH_{cis}H{=}C(CH_3)-$), 6.0−7.3 ppm (br, aromatic protons in polystyrene and poly(*tert*-butylstyrene) units).

Graft Copolymerization of Methacrylate Macromonomers with Methyl Methacrylate. Methacrylate macromonomer (10.1 g), methyl methacrylate (10.737 mL, 10.1 g), and AIBN (40.2 mg) were dissolved in ethyl acetate (90 mL). Nitrogen was bubbled through the solution for 10 min. The reaction proceeded for 48 h at 65 °C (Scheme 1, reaction 3). The graft copolymer was precipitated into methanol. The precipitated graft copolymer was filtered and dried at 100 °C in vacuum for 24 h. The graft copolymers, poly(methyl methacrylate)-*g*-(polystyrene-*b*-poly(*tert*-butylstyrene) (PMMA-*g*-PS-*b*-P*t*BS) and poly(methyl methacrylate)-*g*-(poly(*tert*-butylstyrene)-*b*-polystyrene) (PMMA-*g*-P*t*BS-*b*-PS), were separated from residual methacrylate macromonomer via cyclohexane extraction for 3 days. ^{1}H NMR (400 MHz, $CDCl_3$, δ): 0.6−0.8 ppm (br, $CH_3CH_2CH(CH_3)-$), 0.9−2.5 ppm (br, $-CH_2-$, $-CH_2CH-$, $-C(CH_3)_3$, $-C(CH_3)-$), 3.4−3.9 ppm (br, $-CH_2CH_2OCO-$, CH_3OCO-), 6.0−7.3 ppm (br, aromatic protons in polystyrene and poly(*tert*-butylstyrene) units).

Scheme 1. Synthesis of Selectively-Sulfonated Graft Copolymers[a]

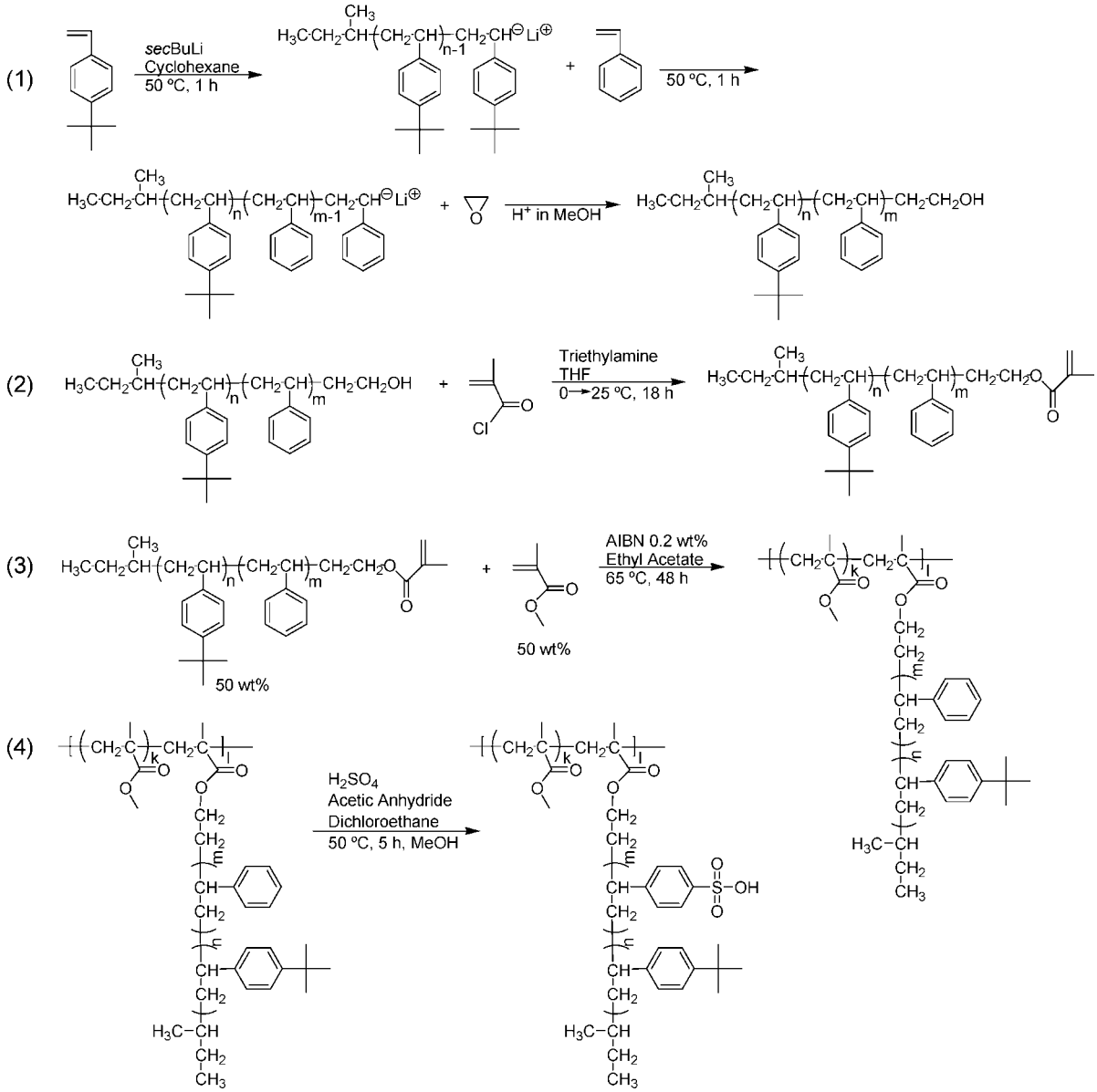

[a] (1) Synthesis of γ-hydroxy-poly(*tert*-butylstyrene-*b*-styrene (P*t*BS-*b*-PS-OH), (2) reaction of P*t*BS-*b*-PS-OH with methacryloyl chloride, (3) graft copolymerization of methyl methacrylate with the methacrylate macromonomer, and (4) sulfonation of the graft copolymers.

Selective Sulfonation and Na^+ Neutralizaton of Graft Copolymers. 2.5 M acetyl sulfate solution was generated via the sequential addition of sulfuric acid (9.3 mL, 0.175 mol) and acetic anhydride (18.9 mL, 0.200 mol) in dichloroethane (41.8 mL) at 0 °C. PMMA-*g*-PS-*b*-P*t*BS (10.5 g) was dissolved in dichloroethane (75.0 mL). Nitrogen was bubbled through the solution for 10 min. The reaction scheme is shown in Scheme 1, reaction 4. The reactor was maintained at 50 °C, and the acetyl sulfate solution (27.1 mL, 2.5 M in dichloroethane) was slowly added. The reaction was allowed to proceed for 5 h at 50 °C until methanol was added to terminate the reaction. The poly(styrenesulfonic acid)-containing graft polymer was first precipitated in a 1:1 mixture of methanol and water, filtered, redissolved in THF, and then precipitated into water. The precipitation and recovery were repeated at least three times. The dried sulfonic acid-containing graft polymer was redissolved in THF, and the acid groups were neutralized with 1 equiv of NaOH solution (1 mol/L). The product polymer was isolated by precipitation into hot water.

Polymer Characterization. ^{1}H NMR spectra of the polymers were obtained on a Varian Unity spectrometer operating at 400 MHz at ambient temperature. Deuterated chloroform (Cambridge Isotope Laboratories) was used as the solvent. Size exclusion chromatography (SEC) measurements were performed in THF at 40 °C at flow rate 1 mL/min using a Waters size exclusion chromatograph equipped with an autosampler, three in-line 5 μm PLgel Mixed-C columns, a Waters 410 refractive index (RI) detector operating at 880 nm, and a miniDAWN multiangle laser light scattering (MALLS) detector operating at 690 nm which was calibrated with narrow polydispersity polystyrene standards. The RI increment (d*n*/d*c*) was calculated online. All reported weight-average molecular weights are absolute molecular weights, which were obtained using the MALLS detector. Glass transition temperatures were determined using a differential scanning calorimeter (DSC) Q200 (TA Instruments) at a heating rate of 10 °C/min under nitrogen. Glass transition temperatures are reported as the onset and the transition midpoint during the second heat.

Morphological Characterization. Solvent-cast films of the graft polymer precursors and the sulfonic acid graft copolymers were prepared from 5 wt % solutions of the polymer in toluene. The solutions were covered to slow solvent evaporation, and films

Table 1. Properties of Hydroxy-Terminated Poly(*tert*-butylstyrene-*b*-styrene) and Poly(styrene-*b*-*tert*-butylstyrene)

	M_n[a]	M_n[b]	M_n PS[a]	M_n PS[b]	M_w/M_n[b]	EO end-capping [%]
P*t*BS-*b*-PS-OH	9740	9670	1020	1790	1.10	100
PS-*b*-P*t*BS-OH	10300	10200	N/A	915	1.07	100

[a] ^{1}H NMR conditions; Varian Unity 400 MHz, $CDCl_3$. [b] Determined using SEC at 40 °C in THF with a MALLS detector.

formed over a period of 20 days. Solvent-cast films of the sodium sulfonate graft copolymers were prepared from 5 wt % polymer MeOH/THF (50/50) solution, and film formation occurred over a period of 2 days. The sodium sulfonate graft copolymers are insoluble in THF, and aprotic solvent needed to be added. The highest solubility of sodium sulfonate graft copolymers were observed in MeOH/THF (50/50). Thin sections of the graft copolymer films (~50 nm) were prepared for TEM by embedding the bulk films in epoxy and ultramicrotoming using a Leica EM-FCS microtome at room temperature. Only the unsulfonated samples were able to be sectioned. The sections were then stained 4 h in OsO_4 vapor. TEM was performed using a JEOL 200CX TEM operated at an accelerating voltage of 120 kV. SAXS data were collected with a customized pinhole collimated 3 m camera. X-rays were generated with a Rigaku Ultrax18 rotating Cu anode generator operated at 45 kV and 100 mA and then filtered with Ni foil to select the Cu Kα doublet (λ = 1.542 Å). Two-dimensional data sets were collected using a Molecular Metrology multiwire area detector, located ~150 cm from the sample. The raw data were corrected for absorption and background noise and then azimuthally averaged. The corrected data were placed on an absolute scale using a sample of type 2 glassy carbon previously calibrated at the Advanced Photon Source, Argonne National Laboratory.

All data reduction and analysis were performed using Igor Pro v5.04B from Wavemetrics, Inc. The features in the scattering data were analyzed by fitting a multivariate model to the data using the least-squares analysis tool in Igor Pro. Bragg diffraction maxima were modeled as Lorentzian (Cauchy) distributions with three variables (amplitude, position, and width). Background functions were usually the sum of a constant (one variable) and a power law (two variables), although for determining peak positions of strong maxima, a linear background function may have been used. Ionomer scattering maxima were fit using the Yarusso−Cooper model with four independent variables, as discussed below. For complex combinations of functions, rather than letting all variables be minimized independently, sections of the data were fitted separately to obtain starting values for subsequent analyses. Where higher order Bragg diffraction maxima were present, the starting values for the distribution centers were taken as the corresponding multiple of the primary Bragg diffraction peak center.

Results and Discussion

Synthesis of Methacrylate Macromonomers. Hydroxy-terminated poly(*tert*-butylstyrene-*b*-styrene) (P*t*BS-*b*-PS-OH) and hydroxy-terminated poly(styrene-*b*-*tert*-butylstyrene) (PS-*b*-P*t*BS-OH), containing 1000 g/mol polystyrene block and 9000 g/mol poly(*tert*-butylstyrene) block, were synthesized via living anionic polymerization and end-capping of the living styryl anions with ethylene oxide. The structural characterization of the diblock copolymers are summarized in Table 1. Molecular weights (M_n from NMR and SEC) of the diblock copolymers ranged from 9500 to 10 300 g/mol with narrow molecular weight distributions (M_w/M_n) 1.07−1.10. Based on the integration of the ^{1}H NMR resonance for the methylene adjacent to the hydroxyl at 3.2−3.4 ppm to the integration of the ^{1}H NMR resonance for the two methyls in the s*ec*-butyl fragment at 0.6−0.8 ppm, 100% end-capping to the terminal hydroxyl group was obtained for all diblock copolymers. The hydroxyl end groups of the diblock copolymers (P*t*BS-*b*-PS-OH and PS-*b*-P*t*BS-OH) were reacted with methacryloyl chloride to produce methacrylate macromonomers (P*t*BS-*b*-PS-methacrylate and PS-*b*-P*t*BS-methacrylate). Conversion of hydroxyl groups to methacrylate groups ranged from 80 to 87% based on the analysis of the shift of the alcohol methylene resonance at 3.2−3.4 ppm to ester methylene resonance at 3.7−4.1 ppm. Thus, the functionality of the methacrylate macromonomers was 0.80−0.87.

Graft Copolymerization of Methacrylate Macromonomer with MMA and Subsequent Sulfonation of Polystyrene Blocks. Graft copolymerization of methacrylate macromonomer with MMA via free radical copolymerization was performed. The results are summarized in Table 2. Sample A has polystyrene blocks adjacent to the PMMA backbone, and sample B has polystyrene blocks at the branch terminus. The weight-average molecular weights were ~200 000 g/mol, and the polydispersity indices were near 2.0. Representative SEC traces of a graft copolymer and a macromonomer are shown in Figure 2. All SEC results showed a monomodel signal, indicating that the cyclohexane extraction quantitatively removed residual macromonomer. Isolated yields were 60−66%, and based on final composition, macromonomer conversion was 43−56%. In the ^{1}H NMR spectrum of the graft copolymers, integrations of the aromatic region (6.0−7.3 ppm) and methyl esters in PMMA (3.4−3.9 ppm) determined the molar ratio of PMMA to macromonomer. On the basis of the polymer composition from ^{1}H NMR and molecular weight of the graft copolymers using SEC, average numbers of branches (λ) of the graft copolymers were calculated and listed in Table 2. The graft copolymers contained 9−10 branches on average. The wt % and the volume fractions of polystyrene (PS) block in the graft copolymers were ~4 wt % and 0.04, respectively.

Site-specific sulfonation of PS blocks with acetyl sulfate solution was performed, and the sulfonic acid content was determined via acid−base titration. All graft copolymers were 100% sulfonated of the polystyrene block based on titration results. Thus, ~4 wt % of the graft copolymer was precisely sulfonated, as shown in Figure 1. The sulfonic acid graft copolymers, poly(methyl methacrylate)-*g*-(sulfonated polystyrene-*b*-poly(*tert*-butylstyrene)) (PMMA-*g*-SPS-*b*-P*t*BS) and poly(methyl methacrylate)-*g*-(poly(*tert*-butylstyrene)-*b*-sulfonated polystyrene) (PMMA-*g*-P*t*BS-*b*-SPS), were successfully synthesized. Finally, a portion of the sulfonic acid graft copolymers, both PMMA-*g*-SPS-*b*-P*t*BS (A) and PMMA-*g*-P*t*BS-*b*-SPS (B) were neutralized with NaOH to produce sodium sulfonate graft copolymers, poly(methyl methacrylate)-*g*-(sodium sulfonate polystyrene-*b*-poly(*tert*-butylstyrene) (PMMA-*g*-NaSPS-*b*-P*t*BS) and poly(methyl methacrylate)-*g*-(poly(*tert*-butylstyrene)-*b*-sodium sulfonate polystyrene) (PMMA-*g*-P*t*BS-*b*-NaSPS). The equivalent weight (EW) of PMMA-*g*-SPS-*b*-P*t*BS (A) and PMMA-*g*-P*t*BS-*b*-SPS (B), which is defined as the weight of polymer per mole of sulfonic acid groups, was estimated to be approximately 2200 g/mol (A) and 2700 g/mol (B), respectively, although the distribution of ionic species in these samples is not random and the EW measure is not very helpful in describing the salient characteristics of these block-specific sulfonated copolymers.

Nonsulfonated graft copolymers, sulfonic acid graft copolymers, and sodium sulfonate graft copolymers were characterized using DSC, SAXS, and TEM, and the influence of relative location of sulfonated blocks in the graft copolymer architecture will be discussed. For simplicity, nonsulfonated graft copolymers A and B will be referred to as A_G and B_G, sulfonic acid graft copolymers will be referred to as A_H and B_H, and sodium sulfonate graft copolymers will be referred to as A_{Na} and B_{Na}.

Thermal Characterization. Glass transition temperatures (T_g) of PMMA-*g*-PS-*b*-P*t*BS (A_G), PMMA-*g*-P*t*BS-*b*-PS (B_G), PMMA-*g*-SPS-*b*-P*t*BS (A_H), PMMA-*g*-P*t*BS-*b*-SPS (B_H),

Table 2. Properties of Graft Copolymers (f = Volume Fraction)

	no. of branches λ	PMMA [wt %]	P*t*BS [wt %]	PS [wt %]	PMMA f	P*t*BS f	PS f	M_w[a]	M_w/M_n[a]
A	9	58.0	37.9	4.1	0.53	0.43	0.04	176 000	2.22
B	10	54.0	42.2	3.8	0.49	0.47	0.04	234 000	1.86

[a] Determined using SEC at 40 °C in THF with a MALLS detector.

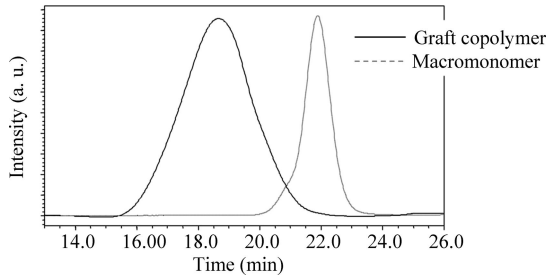

Figure 2. SEC traces of a graft copolymer, PMMA-*g*-P*t*BS-*b*-PS, and a macromonomer, PS-*b*-P*t*BS-methacrylate. SEC conditions: at 40 °C in THF with RI and MALLS detector.

Table 3. Glass Transition Temperatures (T_g) of PMMA-*g*-PS-*b*-P*t*BS (A_G), PMMA-*g*-P*t*BS-*b*-PS (B_G), PMMA-*g*-SPS-*b*-P*t*BS (A_H), PMMA-*g*-P*t*BS-*b*-SPS (B_H), PMMA-*g*-NaSPS-*b*-P*t*BS (A_{Na}), and PMMA-*g*-P*t*BS-*b*-NaSPS (B_{Na})[a]

	T_g (onset) [°C]	T_g (midpoint) [°C]
A_G	122	130
B_G	123	130
A_H	122	131
B_H	128	136
A_{Na}	129	142
B_{Na}	135	151

[a] DSC conditions; TA Instruments Q 200, 10 °C/min second heat.

PMMA-*g*-NaSPS-*b*-P*t*BS (A_{Na}), and PMMA-*g*-P*t*BS-*b*-NaSPS (B_{Na}) are shown in Table 3. All the T_gs were determined from the second heating cycle at 10 °C/min. Some of the samples upon the first heating cycle provided two transitions, which were consistent with T_gs of PMMA and P*t*BS. All graft copolymers had a single T_g in the second heating cycle. This suggested that the rapid cooling rate in DSC did not provide sufficient time for microphase separation to occur. Graft copolymers with immiscible blocks such as poly(vinyl acetate)-*g*-poly(dimethylsiloxane) and poly(vinyl acetate)-*g*-polystyrene[5] typically exhibit a T_g for each block. However, the graft copolymers with low χ value blocks such as poly(*n*-butyl acrylate)-*g*-polystyrene have been reported to show a single T_g.[20]

The Gordon−Taylor equation (eq 1) was used to predict the T_g of the graft copolymers. The reference T_gs of poly(methyl methacrylate), poly(*tert*-butylstyrene), and polystyrene were 120, 145, and 100 °C, respectively.[21] The T_gs and the weight fractions of each block in Table 2 were inserted into the Gordon−Taylor equation:

$$\frac{1}{T_g} = \frac{w_{PMMA}}{T_{g,PMMA}} + \frac{w_{PtBS}}{T_{g,PtBS}} + \frac{w_{PS}}{T_{g,PS}} \quad (1)$$

The calculated T_gs of A_G and B_G were 127 and 128 °C, respectively. These T_gs agreed with the experimentally determined T_gs of A_G and B_G, reported in Table 3, suggesting that microphase separation did not occur, resulting in a single glass transition in the second heating cycle.

The T_g values of the sulfonated graft copolymer with sulfonated blocks at the branch terminus (B_H and B_{Na}) were higher than the T_g values with sulfonated blocks adjacent to the backbone (A_H and A_{Na}). The T_g for the PS block in sulfonated polystyrene block copolymer generally increases with the increase of the degree of the sulfonation (DS).[22−24] For example, the T_g of the sulfonated polystyrene segment of sulfonated poly(styrene-*b*-[ethylene-*co*-butylene]-*b*-styrene) was reported to increase from 82 to 92 °C when DS increased from 2.8 to 14.3%.[22] The T_g of SPS block of sulfonated poly([vinylidene difluoride-*co*-hexafluoropropylene]-*b*-styrene) increased from 86 to 166 °C when DS increased from 0 to 40%.[24] The increase of T_g is associated with ion content and the ionomeric effect. Small regions of restricted mobility are known to act as physical cross-links and raise T_g.[23,25] In this study, the relative location of the sulfonated block was presumed to affect T_g values since the sulfonated graft copolymers possessed similar DS. The higher T_g values of B_H and B_{Na} suggested that the sulfonated blocks at the branch terminus more easily formed ionic interactions. The mobility of the sulfonated blocks on the branch terminus of B_H and B_{Na} presumably enabled more sulfonated blocks to interact and produce ionic aggregates. The sulfonated blocks on the graft branches of A_H and A_{Na} were presumed to be less mobile due to the adjacent backbone and P*t*BS segments, preventing dense ionic associations to occur.

Table 4. χ values for Each Component between PMMA, PS, P*t*BS, and SPS at T = 298 K

$\chi_{PMMA/PS}$	$\chi_{PMMA/PtBS}$	$\chi_{PtBS/PS}$	$\chi_{PMMA/SPS}$	$\chi_{PtBS/SPS}$
0.00565	0.135	0.221	10.4	18.0

Morphological Characterization. It has been reported that the constituting unit of a graft copolymer, rather than the entire polymer, controls the morphological behavior of graft copolymers.[5−7,26,27] Phase behavior of graft copolymer systems depends on the volume fraction of the component and $\chi N/\lambda$, where χ is Flory−Huggins interaction parameter, N is the total degree of polymerization, and λ is the number of branches per graft copolymer.[5] The values of χ were estimated from the molar volumes and the polymer solubility parameters via eq 2:

$$\chi_{12} = \frac{V_0(\delta_2 - \delta_1)^2}{RT} \quad (2)$$

where V_0 is the molar volume, δ_1 and δ_2 the solubility parameters of the respective polymer components, R the gas constant, and T the temperature. V_0 was calculated from $V_0 = (V_1V_2)^{1/2}$, where V_1 and V_2 are the molar volumes of the respective components.[5] The molar volumes of PMMA, P*t*BS, PS, and SPS are 85.6, 168.7, 99.0,[28] and 129.1 cm^3/mol,[28] respectively, where the molar volume for SPS was calculated using addition principle of the group contributions and the atomic contributions.[28] The solubility parameters of PMMA, P*t*BS, PS, and SPS are 18.27,[21] 16.60,[21] 18.66,[21] and 33.96 (J/cm^3)$^{1/2}$,[29,30] respectively, where the solubility parameter for P*t*BS was calculated using addition principle of the molar attraction constant.[21] The calculated χ values at T = 298 K are summarized in Table 4. The large difference of the solubility parameters between SPS and the other components led to very large values of $\chi_{PMMA/SPS}$ and $\chi_{PtBS/SPS}$. This trend agreed well with the trend of $\chi_{PS/SPS}$ in the literature.[31,32] Beck Tan et al. reported $\chi_{PS/SPS}$ was at least 5.6,[31] and Winey et al. concluded $\chi_{PS/SPS}$ was always greater than 25.[32] The calculated results for $\chi N/\lambda$ of the PMMA-*g*-PS-*b*-P*t*BS (A_G), PMMA-*g*-P*t*BS-*b*-PS (B_G), PMMA-*g*-SPS-*b*-P*t*BS (A_H), and PMMA-*g*-P*t*BS-*b*-SPS (B_H) at 298 K are tabulated in Table 5. In A_G and B_G, PMMA/P*t*BS and P*t*BS/PS phases possess $\chi N/\lambda$ = 13.4−25.5, within the weak segregation limit, whereas the $\chi N/\lambda$ = 0.63 and 0.79 of PMMA/PS phase is too low to cause microphase separation. Disordered mi-

Table 5. Estimation of $\chi N/\lambda$ Values for the PMMA-*g*-PS-*b*-P*t*BS (A_G), PMMA-*g*-P*t*BS-*b*-PS (B_G), PMMA-*g*-SPS-*b*-P*t*BS (A_H), and PMMA-*g*-P*t*BS-*b*-SPS (B_H) at $T = 298$ K

	$\chi_{PMMA/PS}N/\lambda$	$\chi_{PMMA/PtBS}N/\lambda$	$\chi_{PtBS/PS}N/\lambda$	$\chi_{PMMA/SPS}N/\lambda$	$\chi_{PtBS/SPS}N/\lambda$
A	0.63	20.9	13.4	1173	1622
B	0.79	25.5	14.7	979	1193

crophase-separated morphologies were expected for A_G and B_G since PMMA and P*t*BS were the dominant components, with volume fraction PMMA 0.49−0.53 and P*t*BS 0.43−0.47, which are shown in Table 2. On the other hand, extremely large $\chi N/\lambda$ values of PMMA/SPS and P*t*BS/SPS phases in A_H and B_H suggested that introduction of sulfonic acid groups would lead to very strong phase separation. The extent of the microphase separation and the morphologies of these graft copolymers were characterized using SAXS and TEM.

SAXS is a powerful tool for determining the long-range structure within polymeric structures.[33,34] Scattering of X-rays by ordered structures generates data in the form of a Fourier transform of the morphology of the sample, and while the loss of morphological information due to the squaring of the scattering amplitude function requires the collection of additional morphological information to draw definitive conclusions, the ability to examine a large sample volume makes SAXS an appealing technique for characterizing bulk morphology. SAXS is an appropriate characterization technique to observe the influence of relative location of sulfonated blocks with constant sulfonation level, 4 wt %, in the sulfonated graft copolymers.

SAXS data for graft copolymers (A_G and B_G) that were prepared from 5 wt % solutions of the polymer in toluene are shown in Figure 3. Absolute scattering intensity was plotted versus the magnitude of the scattering vector, q, where $q = 2\pi \sin(\theta)/\lambda$, and 2θ is the scattering angle. The Bragg spacings, d, were calculated from the primary Bragg maxima as $d = 2\pi/q$ and are listed in Table 6. The data for sample A_G clearly show multiple Bragg reflections, evidence of long-range morphological order. For A_G, the ratio q_1:q_2:q_3 was approximately 1:2:3, consistent with the expected lamellar morphology. The SAXS data for B_G exhibited a very weak increase in scattered intensity at $q \approx 2q_1$ (as indicated by the red arrow in Figure 3), implying that a very poorly formed lamellar morphology might be present. It should be noted that these films were prepared with a very slow evaporation rate (20 days) to obtain morphologies more

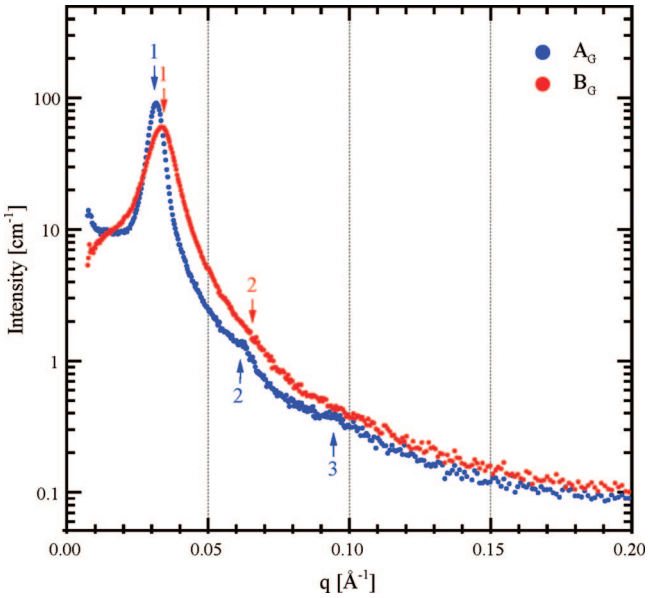

Figure 3. SAXS profiles for PMMA-*g*-PS-*b*-P*t*BS (A_G) and PMMA-*g*-P*t*BS-*b*-PS (B_G).

Table 6. Physical Properties of Graft Copolymers, Sulfonic Acid, and Sodium Sulfonated Graft Copolymers Investigated in SAXS

	q_1 maxima (=q^*) [Å^{-1}]	q/q^*	d [nm][a]	morphology
A_G	0.0316	1, 2, 3	19.9	lamellar
B_G	0.0334	1, 2	18.8	lamellar
A_H	0.0279	1, 2	22.5	lamellar
B_H	0.0310	1, 2	20.2	lamellar + ionic aggregates
A_{Na}	0.0413	1, 2	15.2	lamellar
B_{Na}	0.0397	1	15.8	ionic aggregates

[a] Primary SAXS reflection, $d = 2\pi/q^*$.

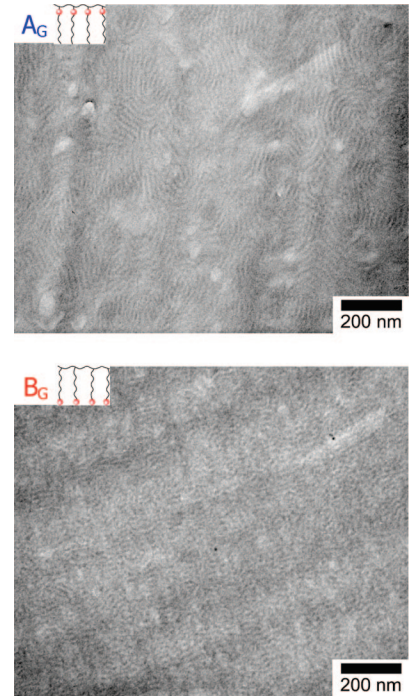

Figure 4. TEM micrographs of PMMA-*g*-PS-*b*-P*t*BS (A_G) and PMMA-*g*-P*t*BS-*b*-PS (B_G).

equilibrium in character. The SAXS data for A_G and B_G, which were cast quickly from THF, each showed only a single scattering maximum. The lack of higher order reflections from THF cast films proved that the slow film formation process promoted self-assembly.

Figure 4 shows TEM micrographs from samples A_G and B_G. The micrograph of A_G shows a lamellar morphology with both domains having approximately equal thicknesses. TEM micrograph of B_G shows microphase separation into a poorly ordered morphology in which some regions appear to have a lamellar character. These observations from TEM are in agreement with the analysis of the SAXS data in Figure 3. The lamellar periods of A_G and B_G from TEM micrographs are approximately 17 ± 2 and 16 ± 2 nm, respectively. The lamellar spacings are in good agreement with the Bragg spacings, given in Table 6, as determined from the SAXS data. PMMA and P*t*BS blocks should have a dominant contribution to the morphology, and the expected morphology would be lamellar based on the volume fraction of PMMA and P*t*BS, 0.43−0.53, in Table 3 and $\chi_{PMMA/PtBS}N/\lambda$, 20.9 or 25.5, in Table 5. $\chi_{PMMA/PtBS}N/\lambda = 20.9$ or 25.5 large enough to possess distinctive microphase separation in comparison with the order−disorder transition boundary for comb copolymers with randomly placed graft junctions, approximately $\chi N/\lambda = 10$.[27]

The different morphological behaviors of A_G and B_G are determined by a balance between relatively weak driving forces for microphase separation and self-assembly. The main difference between A_G and B_G is the location of PS blocks, and

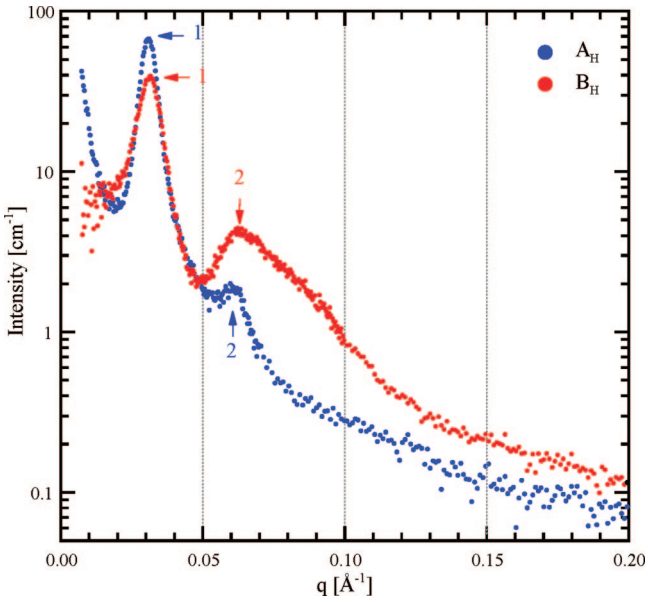

Figure 5. SAXS profiles for sulfonic acid graft copolymers PMMA-*g*-SPS-*b*-P*t*BS (A_H) and PMMA-*g*-P*t*BS-*b*-SPS (B_H).

because there is a significant difference between the χ values for the interactions between PS, PMMA, and P*t*BS, this difference in architecture has a critical effect. In the A_G copolymer, because the PS blocks are located adjacent to the PMMA backbone and are nearly miscible with PMMA ($\chi_{PMMA/PS} = 0.005\,65$), the strong repulsive forces between P*t*BS and both PS ($\chi_{PtBS/PS} = 0.221$) and PMMA ($\chi_{PMMA/PtBS} = 0.135$) combine to dominate the morphological behavior. These interactions push the morphological behavior into the weak segregation regime and a lamellar morphology is formed ($\chi_{PMMA/PtBS}N/\lambda = 20.9$ and $\chi_{PtBS/PS}N/\lambda = 13.4$). In the B_G copolymer, however, the PS is located at the end of the grafts, away from the PMMA backbone, dramatically impeding the ability of the graft copolymer to microphase separate and form an ordered morphology. Although the P*t*BS blocks are strongly immiscible with the PMMA backbone, they are also strongly repelled by the PS blocks at the end of the grafts. Combined with the near miscibility of the PS and PMMA blocks, the formation of microphase-separated domains containing both PS and P*t*BS is strongly inhibited. As a result, the morphology of B_G, as shown in Figure 4, is microphase-separated, but with poorly ordered, frustrated lamellar domains.

Sulfonation of these complex graft copolymers further complicates their morphological behavior. SAXS profiles for sulfonic acid graft copolymers (A_H and B_H) that were cast from 5 wt % solutions of the polymer in toluene are shown in Figure 5. Two Bragg reflections in the SAXS data for A_H indicate that this material retains its lamellar morphology, although with a slight decrease in long-range order. The maxima positions q_1 and q_2 and the Bragg spacings, d, are summarized in Table 6. The data for sample B_H show two maxima, but the shape of the second maximum is unusually broad and was not fit well with a single Lorentzian or Gaussian distribution as would be the case for a Bragg reflection. If the angle at which the maximum intensity of the second scattering maximum for B_H is taken as q_2, then B_H also exhibits a 2:1 ratio of scattering maxima value, again consistent with the predicted lamellar morphology.

Because of the extremely brittle nature of sulfonated samples, TEM data were not obtained. However, for both A_H and B_H, the SAXS data (Figure 5) show clear and noteworthy differences from that obtained for A_G and B_G. In both A_H and B_H, the poly(styrenesulfonic acid) (SPS) blocks comprise only 4 wt % of each graft copolymer, but because of the strong enthalpic repulsion between the SPS and both PMMA and P*t*BS ($\chi_{PMMA/SPS} = 10.4$ and $\chi_{PtBS/SPS} = 18.0$), the morphological behavior as deduced from the SAXS data is significantly altered. First, quick casting from THF was sufficient to produce well-ordered lamellar microphase separation, a marked contrast from the behavior of the THF-cast A_G and B_G. Second, for A_H, the location of the SPS block at the PMMA backbone has an effect similar to the location of the P*t*BS block at the backbone in B_G, creating a situation where the block grafted to the backbone is strongly driven to microphase separate both from the backbone and the end of the graft. In the case of A_H, the underlying lamellar morphology of the graft copolymer is only somewhat disrupted, with only two Bragg maxima observed in SAXS, rather than the three maxima observed for A_G (Figure 3). Third, the lamellar period of A_H (22.4 nm) is slightly larger than that for A_G (19.6 nm), a natural result of the addition of bulky sulfonic acid groups to the PS block and possibly indicative of water uptake.

The effect of sulfonating the PS block is much more profound for the B architecture (B_H). Instead of the single SAXS maximum observed for B_G, a large, broad second maximum is observed. The unusual shape of the second maximum in sample B_H was estimated to be a combination of a second-order Bragg reflection, located around $q \approx 2q_1$, and a third feature in the scattering data. The molecular architecture of this sample, with sulfonated PS blocks at the end of the grafts, makes the formation of ionic aggregates such as those observed in ionomers very likely. SAXS data for such ionomers are characterized by a strong "ionomer peak", usually attributed to interparticle scattering between aggregates of ionic functional groups, and generally fit using the Yarusso−Cooper (YC) model.[35]

The YC model treats the ionic aggregates as spherical particles with an ionic core having radius R_1. The ionic aggregates are not allowed to come into contact with each other, using the approach of Guinier and Fournet to include liquidlike ordering of the aggregates in the sample.[34] A shell of restricted mobility with radius R_{CA} definedfrom the center of each aggregate, where the closest approach distance between two aggregates is $2R_{CA}$. The average sample volume per aggregate is defined as V_p. In this model, the X-ray scattering intensity is represented by

$$I(q) = I_e(q)V\frac{1}{V_p}V_1^2\rho_1^2\Phi^2(qR_1)\frac{1}{1+\left(\frac{8\,V_{CA}}{V_p}\right)\epsilon\,\Phi(2qR_{CA})} \quad (3)$$

$$V_{CA} = \frac{4}{3}\pi R_{CA}^3 \quad (4)$$

$$V_1 = \frac{4}{3}\pi R_1^3 \quad (5)$$

$$\Phi(x) = 3\,\frac{\sin x - x\cos x}{x^3} \quad (6)$$

where $I(q)$ is the observed intensity and $I_e(q)$ is the intensity scattered by a single electron under the experimental conditions, V is the volume of the sample, ρ_1 is the electron density difference between the matrix and the ionic aggregate, and ϵ is a constant close to unity. Because $I_e(q)$ can be regarded as a constant, the term $I_e(q)V\rho_1^2$ can be viewed as a single adjustable parameter. Thus, the model has four fitting parameters: R_1, R_{CA}, V_p, and $I_e(q)V\rho_1^2$. By fitting calculated scattering data to the experimental data, one can determine a combination of the four most probable fitting parameters, describing the characteristics of ionic aggregates in the sample.[35–38]

The result of fitting the YC model to the ionomer peak in the SAXS data for PMMA-*g*-P*t*BS-*b*-SPS (B_H) is shown in

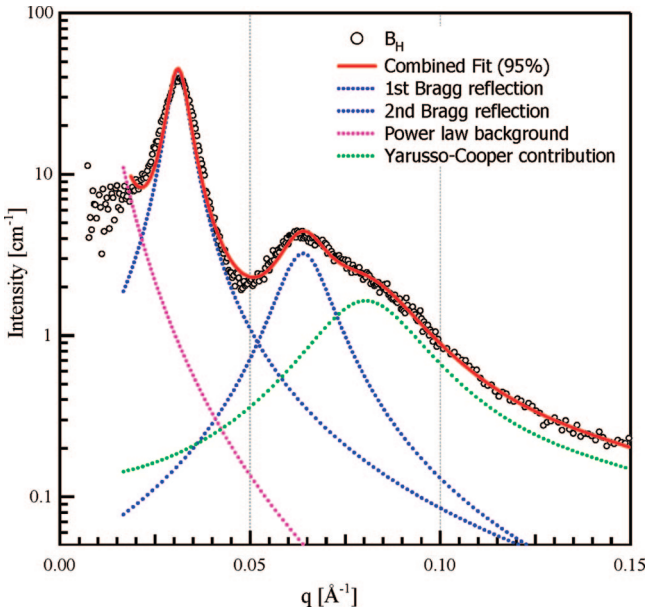

Figure 6. Fitting SAXS ionomer peak of PMMA-*g*-P*t*BS-*b*-SPS(B_H) to the Yarusso−Cooper model.

Table 7. Best-Fit Parameters of the Yarusso−Cooper Model for the Ionomer Peak

	R_1 (Å)	R_{CA} (Å)	V_p (Å^3)	$R_{CA} - R_1$ (Å)	V_1 (Å^3)	V_p^{-1} (Å^{-3})	V_1/V_p
B_H	19	35	2.0×10^5	16	2.9×10^4	4.9×10^{-6}	0.14
B_{Na}	30	38	2.5×10^5	8	1.1×10^5	4.0×10^{-6}	0.45

Figure 6. Lorentzian distributions were used for the primary Bragg maximum and for a secondary Bragg maximum centered at approximately $2q_1$. The significantly diminished intensity of the second-order reflection relative to the primary Bragg reflection, in addition to the increase in peak width, is consistent with typical scattering data from lamellar materials with moderate long-range order. The YC model was used to add a contribution from ionic aggregates to the second maximum in the data, which has a shape expanded beyond the second Lorentzian. This approach generated hypothetical scattering data that fit the main features of the SAXS data very well, particularly the slight dip in scattered intensity between $q_2 = 0.06$ Å^{-1} and $q = 0.085$ Å^{-1}, where the contributions from the second Bragg maximum and the ionomer peak overlap. The YC fitting parameters for the ionomer peak are summarized in Table 7.

The SAXS data for the sodium sulfonate graft copolymers (A_{Na} and B_{Na}), prepared from THF/MeOH solutions, are shown in Figure 7. For sample A_{Na} they show multiple Bragg reflections for which the ratio of scattering angles follows q_1: q_2 = 1:2, indicating a lamellar morphology. When compared to the scattering data for A_H, the peaks for A_{Na} appear to have been broadened by neutralization of the copolymer with sodium, indicating the formation of a less well-ordered microstructure. This observation agrees with Weiss' findings that the SAXS reflections broadened as the ionic interactions increased (i.e., as the cation was changed from H^+ to Zn^{2+} to Na^+, the morphology became less ordered).[39,40] The degree of ordering of the block copolymer morphology should depend on the strength of the ion-dipole interactions since the relaxation behavior of the dipolar interactions dictates the local viscosity of the medium.[40] The lamellar periods, d, of the sodium sulfonate graft copolymers were only 15.2 nm for A_{Na} and 15.8 nm for B_{Na}, significantly less than those measured for either A_G and B_G or the acid forms A_H and B_H, confirming that the strong ionic interactions with the Na^+ counterions have a dominant effect on morphology. The change of the Bragg

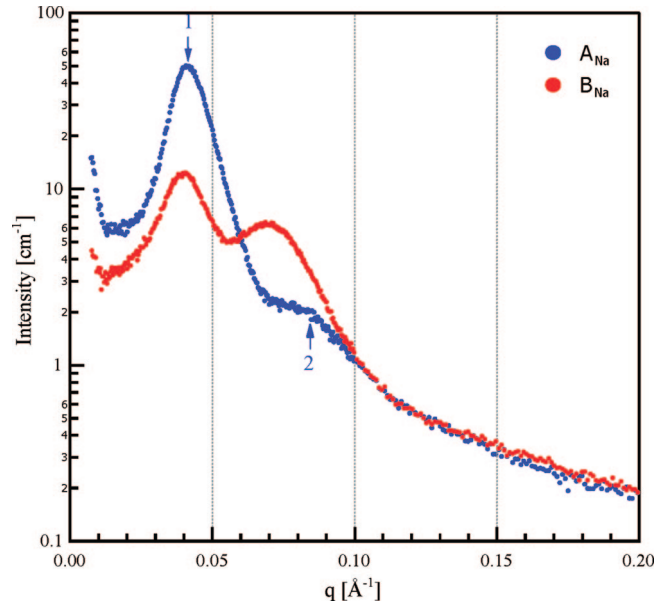

Figure 7. SAXS profiles for sodium sulfonate graft copolymers PMMA-*g*-NaSPS-*b*-P*t*BS (A_{Na}) and PMMA-*g*-P*t*BS-*b*-NaSPS (B_{Na}) prepared from THF/MeOH.

spacings, d, upon neutralization derived from shifting scattering maxima in SAXS profiles. The positions of the primary Bragg maxima were shifted to higher q value upon neutralization.

The scattering data for the second sodium neutralized copolymer, B_{Na}, does not present scattering data typical of lamellar microphase-separated block copolymer morphologies. The second maximum is unusually strong and broad. In addition, a third-order reflection is also absent, which would be expected given the intensity of the second-order reflection. As was seen for B_H, the molecular architecture of this sample, with sulfonated PS blocks at the branch termini, appears to promote the formation of ionic aggregates. Therefore, the same approach used to model the scattering data for B_{Na} was used for B_H, where the second maximum was modeled as an ionomer peak using the YC model.

The calculated scattering data fit to the SAXS data collected for PMMA-*g*-P*t*BS-*b*-NaSPS (B_{Na}) are shown in Figure 8. The second maxima (ionomer scattering maxima) were fitted using the YC model. A reasonable fit is obtained when the YC model is used to fit the second maximum while a Lorentzian is used for the primary scattering maximum, supporting the hypothesis that the second maximum is due primarily to the presence of ionic aggregates.

The fitting parameters for B_{Na} from the YC model are summarized in Table 7. R_1 increases upon neutralization, while R_{CA} remains constant. This leads to a decrease in the thickness of the restricted mobility layer $R_{CA} - R_1$. V_1 increased due to the increase of R_1, indicating that the size of the ionic aggregates increased upon neutralization. The number density of scattering particles ($1/V_p$) was almost constant. The volume fraction of aggregates in the sample, V_1/V_p, increased upon neutralization. A sodium counterion is larger than a proton counterion, which may lead to the increase of V_1 and V_1/V_p. The increase of the number of sodium sulfonate blocks (the increase of the number of sodium sulfonate graft copolymers) per an aggregate might also lead to the increase of V_1 and V_1/V_p.

Conclusions

Novel selectively sulfonated graft copolymers, PMMA-*g*-(SPS-*b*-P*t*BS) and PMMA-*g*-(P*t*BS-*b*-SPS), were successfully

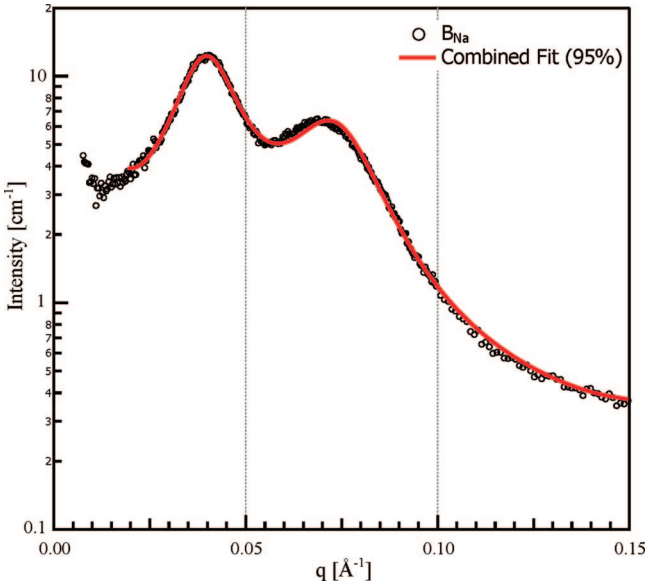

Figure 8. Fitting SAXS ionomer peak of PMMA-*g*-P*t*BS-*b*-SNaPS(B_{Na}) to the Yarusso−Cooper model.

synthesized and characterized via DSC, SAXS, and TEM. The graft copolymers contained approximately 9−10 branches on average and 4 wt % of sulfonic acid or sodium sulfonate blocks. The location of the sulfonated blocks, either adjacent to the backbone or at the branch termini, was determined from the molecular architecture of the starting graft copolymer. The thermal properties of the site-specifically sulfonated graft copolymers were characterized using DSC, and a single glass transition temperature was observed. The sulfonated graft copolymer with sulfonated blocks at the branch terminus (B_H and B_{Na}) had higher T_g values than those with sulfonated blocks adjacent to the backbone (A_H and A_{Na}). The trend of higher T_gs indicated that sulfonated graft copolymer B enabled more sulfonated blocks to interact due to the mobility of the sulfonated blocks at the graft ends. SAXS data for the nonsulfonated graft copolymers (A_G and B_G), sulfonic acid graft copolymers (A_H and B_H), and sodium sulfonate graft copolymers (A_{Na}) showed the Braggs reflections indicative of lamellar morphologies. TEM confirmed the lamellar morphology of A_G and lamellar-type morphology of B_G. Both χ and $\chi N/\lambda$ values were used to predict the phase behavior of the ordered morphologies considering the location of each block. The expected morphologies from χ and $\chi N/\lambda$ values were consistent with the observed morphologies.

The SAXS data for the sulfonated graft copolymers with the B architecture revealed an ionomer peak whereas the sulfonated graft copolymers with the A architecture did not show evidence of ionic aggregates. The presence of ionomer peaks in the B samples was consistent with the observation of strong ionic interaction in T_g analysis. The scattering from the ionic aggregates was characterized using the YC model. The best-fit parameters via the YC model suggested an increase of the size of the ionic aggregates and decrease of the restricted mobility layer upon neutralization.

The observation of resolved ionomer peaks in the scattering data for the samples with a B-type molecular architecture (B_H and B_{Na}) illustrated that the balance between molecular architecture and microphase separation in these materials was not strictly dominated by large enthalpic repulsion of the SPS from the other blocks. Placing the sulfonated block at the branch terminus allowed the formation of ionic aggregates due to the mobility of the branch ends, while copolymers with the sulfonated blocks close to the polymer backbone exhibited little insignificant formation of ionic aggregates. Thus, while the calculated values of the Flory−Huggins parameter for SPS and the blocks are remarkable, it is clear from these experiments that molecular architecture plays a significant morphological role and can be used as a design parameter for utilization of ionomers.

Acknowledgment. This material is based upon work funded by the U.S. Army Research Laboratory and the U.S. Army Research Office under grant DAAD19-02-1-0275 Macromolecular Architecture for Performance (MAP) MURI. The authors acknowledge unrestricted complementary funding from Kraton Polymers LLC and insightful discussions with Dr. Carl Willis.

References and Notes

(1) Jenkins, D. W.; Hudson, S. M. *Chem. Rev.* **2001**, *101* (11), 3245–3273.
(2) Hadjichristidis, N.; Pitsikalis, M.; Iatrou, H.; Pispas, S. *Macromol. Rapid Commun.* **2003**, *24* (17), 979–1013.
(3) Ito, K. *Prog. Polym. Sci.* **1998**, *23* (4), 581–620.
(4) Yang, Y.; Holdcroft, S. *Fuel Cells* **2005**, *5* (2), 171–186.
(5) Maynard, H. D.; Lyu, S. P.; Fredrickson, G. H.; Wudl, F.; Chmelka, B. F. *Polymer* **2001**, *42* (18), 7567–7574.
(6) Beyer, F. L.; Gido, S. P.; Buschl, C.; Iatrou, H.; Uhrig, D.; Mays, J. W.; Chang, M. Y.; Garetz, B. A.; Balsara, N. P.; Tan, N. B.; Hadjichristidis, N. *Macromolecules* **2000**, *33* (6), 2039–2048.
(7) Xenidou, M.; Beyer, F. L.; Hadjichristidis, N.; Gido, S. P.; Tan, N. B. *Macromolecules* **1998**, *31* (22), 7659–7667.
(8) Chuy, C.; Ding, J. F.; Swanson, E.; Holdcroft, S.; Horsfall, J.; Lovell, K. V. *J. Electrochem. Soc.* **2003**, *150* (5), E271−E279.
(9) Ding, J. F.; Chuy, C.; Holdcroft, S. *Macromolecules* **2002**, *35* (4), 1348–1355.
(10) Hickner, M. A.; Ghassemi, H.; Kim, Y. S.; Einsla, B. R.; McGrath, J. E. *Chem. Rev.* **2004**, *104* (10), 4587–4611.
(11) Harrison, W. L.; Hickner, M. A.; Kim, Y. S.; McGrath, J. E. *Fuel Cells* **2005**, *5* (2), 201–212.
(12) Schulz, G. O.; Milkovich, R. *J. Appl. Polym. Sci.* **1982**, *27* (12), 4773–4786.
(13) Balastre, M.; Li, F.; Schorr, P.; Yang, J.; Mays, J. W.; Tirrell, M. V. *Macromolecules* **2002**, *35* (25), 9480–9486.
(14) Guenoun, P.; Davis, H. T.; Tirrell, M.; Mays, J. W. *Macromolecules* **1996**, *29* (11), 3965–9.
(15) Toomey, R.; Mays, J.; Holley, D. W.; Tirrell, M. *Macromolecules* **2005**, *38* (12), 5137–5143.
(16) Valint, P. L.; Bock, J. *Macromolecules* **1988**, *21* (1), 175–179.
(17) Yang, J. C.; Jablonsky, M. J.; Mays, J. W. *Polymer* **2002**, *43* (19), 5125–5132.
(18) Yang, J. C.; Mays, J. W. *Macromolecules* **2002**, *35* (9), 3433–3438.
(19) Zhang, Y.; Tirrell, M.; Mays, J. W. *Macromolecules* **1996**, *29* (22), 7299–7301.
(20) De la Fuente, J. L.; Fernandez-Garcia, M.; Madruga, E. L. *J. Appl. Polym. Sci.* **2001**, *80* (5), 783–789.
(21) Brandrup, J.; Immergut, E. H. *Polymer Handbook*, 3rd ed.; Wiley: New York, 1989.
(22) Mauritz, K. A.; Blackwell, R. I.; Beyer, F. L. *Polymer* **2004**, *45* (9), 3001–3016.
(23) Mokrini, A.; Del Rio, C.; Acosta, J. L. *Solid State Ionics* **2004**, *166* (3−4), 375–381.
(24) Shi, Z. Q.; Holdcroft, S. *Macromolecules* **2005**, *38* (10), 4193–4201.
(25) Eisenberg, A.; Hird, B.; Moore, R. B. *Macromolecules* **1990**, *23* (18), 4098–4107.
(26) Benoit, H.; Hadziioannou, G. *Macromolecules* **1988**, *21* (5), 1449–1464.
(27) Shinozaki, A.; Jasnow, D.; Balazs, A. C. *Macromolecules* **1994**, *27* (9), 2496–2502.
(28) Van Krevelen, D. W.; Hoftyzer, P. J. *Properties of Polymers*; Elsevier: New York, 1976.
(29) Kim, B.; Kim, J.; Jung, B. *J. Membr. Sci.* **2005**, *250* (1−2), 175–182.
(30) Lu, X. Y.; Weiss, R. A. *Macromolecules* **1996**, *29* (4), 1216–1221.
(31) Tan, N. C. B.; Liu, X.; Briber, R. M.; Peiffer, D. G. *Polymer* **1995**, *36* (10), 1969–1973.
(32) Zhou, N. C.; Xu, C.; Burghardt, W. R.; Composto, R. J.; Winey, K. I. *Macromolecules* **2006**, *39* (6), 2373–2379.
(33) Fairclough, J. P. A.; Hamley, I. W.; Terrill, N. J. *Radiat. Phys. Chem.* **1999**, *56* (1−2), 159–173.
(34) Guinier, A.; Fournet, G. *Small-Angle Scattering of X-rays*; John Wiley & Sons: New York, 1955.

(35) Yarusso, D. J.; Cooper, S. L. *Macromolecules* **1983**, *16* (12), 1871–1880.
(36) Tsujita, Y.; Hayashi, N.; Yamamoto, Y.; Yoshimizu, H.; Kinoshita, T.; Matsumoto, S. *J. Polym. Sci., Part B: Polym. Phys.* **2000**, *38* (10), 1307–1311.
(37) Tsujita, Y.; Yasuda, M.; Takei, M.; Kinoshita, T.; Takizawa, A.; Yoshimizu, H. *Macromolecules* **2001**, *34* (7), 2220–2224.
(38) Wouters, M. E. L.; Goossens, J. G. P.; Binsbergen, F. L. *Macromolecules* **2002**, *35* (1), 208–216.
(39) Lu, X. Y.; Steckle, W. P.; Weiss, R. A. *Macromolecules* **1993**, *26* (24), 6525–6530.
(40) Mani, S.; Weiss, R. A.; Williams, C. E.; Hahn, S. F. *Macromolecules* **1999**, *32* (11), 3663–3670.

MA800178D